Signal Processing 91 (2011) 114–125

Contents lists available at ScienceDirect

Signal Processing

journal homepage: www.elsevier.com/locate/sigpro

Vonn distribution of relative phase for statistical image modeling in complex wavelet domain

An Vo [a,*], Soontorn Oraintara [b], Nha Nguyen [b]

[a] The Feinstein Institute for Medical Research, North Shore LIJ Health System, 350 Community Drive, Manhasset, NY 11030, USA
[b] Department of Electrical Engineering, University of Texas at Arlington, Arlington, TX 76019, USA

ARTICLE INFO

Article history:
Received 2 March 2010
Received in revised form
3 June 2010
Accepted 14 June 2010
Available online 20 June 2010

Keywords:
Relative phase
Probability density function of relative phase
Vonn distribution
Statistical image modeling
Joint distribution of phases
Image retrieval
Complex wavelet transforms

ABSTRACT

With the assumptions of Gaussian as well as Gaussian scale mixture models for images in wavelet domain, marginal and joint distributions for phases of complex wavelet coefficients are studied in detail. From these hypotheses, we then derive a relative phase probability density function, which is called Vonn distribution, in complex wavelet domain. The maximum-likelihood method is proposed to estimate two Vonn distribution parameters. We demonstrate that the Vonn distribution fits well with behaviors of relative phases from various real images including texture images as well as standard images. The Vonn distribution is compared with other standard circular distributions including von Mises and wrapped Cauchy. The simulation results, in which images are decomposed by various complex wavelet transforms, show that the Vonn distribution is more accurate than other conventional distributions. Moreover, the Vonn model is applied to texture image retrieval application and improves retrieval accuracy.

1. Introduction

Many applications in image processing such as image compression, restoration, synthesis, segmentation and retrieval can benefit from a statistical model to characterize images in transform domains. A clean, precise probability model which can sufficiently describe typical images becomes essential. In this paper, a new model for relative phases of complex directional wavelet coefficients is proposed for image modeling, and its application in texture image retrieval is presented.

The statistics of wavelet coefficients have been studied [1,2] and wavelet coefficients within a subband are often assumed to be independent and identically distributed. They can be modeled by a two-parameter generalized Gaussian density (GGD) [1,3–5]. The GGD is a suitable distribution for peaky and heavy-tailed non-Gaussian statistics of wavelet decompositions. Although the GGD wavelet marginal model is more powerful than the Gaussian model, it does not take into account the dependencies between different subbands as well as between a coefficient and its neighboring coefficients in the same subband.

Joint statistical models in the wavelet domain [6–9] then have been developed. A bivariate probability density function has been proposed to model the statistical dependencies between a wavelet coefficient and its parent [9]. The wavelet coefficients within each local neighboring are characterized by Gaussian scale mixture model (GSM), which can capture behaviors of marginal distributions of wavelet coefficients and correlations in their local amplitudes [8]. The hidden Markov model with a two-state hidden multiplier variable was introduced in [6,7] to capture key features of a joint probability density of wavelet coefficients. A continuous multiplier variable has been proposed to governed the local variance [10,11,8,12]. In [8,13], the authors developed a model

* Corresponding author. Tel.: +1 516 562 1071; fax: +1 516 562 1008.
E-mail addresses: anphuocnhu.vo@mavs.uta.edu, avo@nshs.edu (A. Vo).
URL: http://www.naaan.org/anvo/ (A. Vo).

0165-1684/$ - see front matter © 2010 Elsevier B.V. All rights reserved.
doi:10.1016/j.sigpro.2010.06.014

for neighborhoods of oriented pyramid coefficients based on a GSM model which is a product of a Gaussian random vector and an independent hidden random scalar multiplier. This model can account for both marginal and pairwise joint distributions of wavelet coefficients.

In most of the above statistical models, only the real part or the magnitude of wavelet coefficients is modeled and used for image processing applications. One of the earliest works that point out the importance of phase information is [14], with the famous example where the main image structure is reconstructed by using only phases of Fourier coefficients. Phases hold crucial informations about image structures and features. The higher-order Fourier statistics have been then applied to examine the phase structure in natural images [15]. Image features such as edges and shadows are determined by analyzing phases of harmonic components [16] or computing the phase congruency [16–18]. At the points of isolated even and odd symmetric features such as lines and step edges, arrival phases of Fourier harmonics are identical [16,19]. The phase congruency matrix provides a quantitative measure of the significance of an edge at each pixel of images, and yields a high quality in edge detection [17]. The importance of the phase of wavelet coefficients in the dual-tree complex wavelet transform is also presented in [20]. Some previous works have used Gabor phases in image classification applications such as iris and palmprint identification [21,22] and face recognition [23]. These methods are based on the quadrant bit coding (QBC) extracted from complex Gabor coefficients. Each pixel in each subband will be encoded to two bits according to the quadrant in which the Gabor phase angle lies.

Some other applications exploit local phase informations across scales of complex wavelets such as description of texture images [12], detection of blurred images [24], object recognition [25] and face recognition [26]. In [12], local phase behaviors are captured by cross-correlations of complex coefficients of bands at adjacent scales (fine-scale and coarse-scale), and this statistical measurement distinguishes edges from lines and helps in representing gradients due to shading and lighting effects. In [24], a local phase coherence relationship across scales and spaces has been suggested and phases of the finest scale coefficients can be well predicted from phases of the coarser scale coefficients. The disruption of this local phase is an effective measure for blur detection [24]. Across scale relationships are also captured using a modified product of coefficients at adjacent scales and have been used in [25,27]. Another investigation of local phases in the same orientation and the same scale is based on the dual-tree complex wavelet transform (DTCWT) [28] and the complex directional filter bank (CDFB) [29]. The feature orientations are determined by the phase difference between adjacent coefficients in six fixed directional subbands [28] and in 2^n directions [30].

The relative phase of complex wavelet coefficients has been studied and two standard circular distributions including von Mises and wrapped Cauchy have been proposed for relative phase distribution in [31]. Von Mises distribution fits well with the relative phase probability density functions (pdf) which are in Gaussian shapes. However, it is not accurate enough to model peaky and heavy-tailed pdfs. On the contrary, wrapped Cauchy distribution fits well with peaky and heavy-tailed pdfs while it does not fits well with relative phase pdfs in Gaussian shapes [31]. In this paper, marginal and joint distributions of phases of complex wavelet coefficients are studied with the assumptions of Gaussian as well as Gaussian scale mixture models (GSM). We then derive a relative phase pdf called Vonn distribution in Section 2 with the assumption of Gaussian model. The Vonn distribution is proved to be also true with the GSM model in Section 3. In Section 4, we present an algorithm maximizing the likelihood of data under the model to estimate Vonn parameters. Section 5 details a comparison of the Vonn distribution with von Mises and wrapped Cauchy distributions in different complex wavelet transforms. Finally, Section 6 presents the texture image retrieval application and simulation results. The preliminary version of this work is partially described in [32].

2. Derivation of the Vonn distribution of relative phases based on Gaussian model

Our objective is to find a statistical model which is able to accurately capture phase information in the complex wavelet domain, and is also able to sufficiently describe natural images. In this section, with the assumption that distributions of real and imaginary coefficients are two real Gaussian distributions, we study the probability distribution of complex coefficients and the joint distribution of two neighboring phases. From the study results, we then derive a probability density function for relative phases within a particular subband.

2.1. Complex Gaussian distribution of complex wavelet coefficients

By construction of the complex wavelet, each pair of corresponding filters have the Hilbert transform relationship [33]. Therefore, an equivalent directional complex filter for each subband has a one-sided frequency support, and outputs of complex filters are complex coefficients. We assume that real and imaginary coefficients in each subband are normally distributed. This assumption will be relaxed to cover a much broader class of distributions in the next section.

Let $\mathbf{z}=(z_1,z_2)^T$ be a complex random vector, where z_1 represents the reference coefficient, z_2 represents the neighboring coefficient and $\mathbf{z}=\mathbf{x}+j\mathbf{y}$. Hence, $\mathbf{x}=(x_1,x_2)^T$ and $\mathbf{y}=(y_1,y_2)^T$ are two real random vectors normally distributed with a joint density functions $p(\mathbf{x},\mathbf{y})$. Since complex directional filters are bandpass, their DC component is equal to zero. As a result, $E[x_n]=\mathbf{0}$, $E[y_n]=\mathbf{0}$ and $E[z_n]=E[x_n]+jE[y_n]=\mathbf{0}$, where $E[\cdot]$ is the expectation operator and $n=1,2$. Since each pair of complex directional filters have the Hilbert transform relationship, $E[x_n^2]\approx E[y_n^2]$. Therefore $E[\mathbf{z}\mathbf{z}^T]\approx 0$. Furthermore, $\mathbf{C}_z=E[\mathbf{z}\mathbf{z}^H]$ is defined as the complex covariance matrix. In these expressions, the superscript T denotes transposition, the

superscript H denotes complex conjugate transposition, and $j=\sqrt{-1}$.

By definition, $\mathbf{C}_z$ is positive definite and Hermitian symmetric, hence, its inverse exists. Then $p(\mathbf{x},\mathbf{y})$ can be written as a function of $\mathbf{z}$ such as $p(\mathbf{x},\mathbf{y})\equiv p(\mathbf{z})$, where $p(\mathbf{z})$ is a real-valued function of a complex vector $\mathbf{z}$. The density function $p(\mathbf{z})$ is commonly referred to as the complex Gaussian density function and can be written as [34,35]

$$p(\mathbf{z})=\frac{\exp(-\mathbf{z}^H\mathbf{C}_z^{-1}\mathbf{z})}{\pi^2\det(\mathbf{C}_z)}. \tag{1}$$

2.2. Marginal distribution of phases

In stead of decomposing $\mathbf{z}$ into Cartesian coordinates, we can write it in terms of polar coordinates. In 1-D case, let $\mathbf{z}=z_1=r_1e^{j\theta_1}$. In each subband, complex wavelet coefficients have zero mean, i.e. $E[z_1]=0$, and their covariance $\mathbf{C}_z=\psi_{11}$. Then we have the joint distribution of $\mathbf{r}$ and $\mathbf{\Theta}$, $p(\mathbf{r},\mathbf{\Theta})=r_1p(\mathbf{z})$ as

$$p(r_1,\theta_1)=\frac{r_1}{\pi\psi_{11}}\exp\left(-\frac{r_1^2}{\psi_{11}}\right). \tag{2}$$

Hence the marginal distribution of phases can be given by

$$\begin{aligned}p(\theta_1)&=\int_0^\infty\frac{r_1}{\pi\psi_{11}}\exp\left(-\frac{r_1^2}{\psi_{11}}\right)dr_1\\&=\frac{1}{2\pi}.\end{aligned} \tag{3}$$

The uniform distribution of phases agrees with observation in [31].

2.3. Joint distribution of two neighboring phases

From the complex Gaussian model (1), we investigate behaviors of a joint distribution of two neighboring phases in the complex wavelet domain. Let $\mathbf{z}=(z_1,z_2)^T=(r_1e^{j\theta_1},r_2e^{j\theta_2})^T=\mathbf{r}e^{j\mathbf{\Theta}}$, where z_1 represents the reference coefficient, z_2 represents the neighboring coefficient and $(\mathbf{r},\mathbf{\Theta})$ are the polar coordinates of $\mathbf{z}$. Hence, we have the joint distribution $p(\mathbf{r},\mathbf{\Theta})=r_1r_2p_{\mathbf{z}}(\mathbf{z})$ [35] as

$$p(r_1,r_2,\theta_1,\theta_2)=r_1r_2\frac{\exp(-\mathbf{z}^H\mathbf{C}_z^{-1}\mathbf{z})}{\pi^2\det(\mathbf{C}_z)}. \tag{4}$$

In each subband, complex wavelet coefficients have zero mean and their covariance $\mathbf{C}_z=E[\mathbf{z}\mathbf{z}^H]=\left[\begin{smallmatrix}\psi_{11}&\psi_{12}\\ \psi_{12}^*&\psi_{22}\end{smallmatrix}\right]=\mathbf{\Phi}^{-1}$. The matrix $\mathbf{C}_\mathbf{z}$ is a positive definite Hermitian matrix, so its inverse $\mathbf{\Phi}$ exists. Let $\mathbf{\Phi}=\left[\begin{smallmatrix}\varphi_{11}&\varphi_{12}\\ \varphi_{12}^*&\varphi_{22}\end{smallmatrix}\right]$, where $\varphi_{12}=|\varphi_{12}|e^{j\mu_\varphi}$, and the superscript $*$ denotes complex conjugate. Then $\mathbf{z}^H\mathbf{C}_z^{-1}\mathbf{z}=r_1^2\varphi_{11}+r_2^2\varphi_{22}+2\,\mathbf{Re}[r_1r_2|\varphi_{12}|e^{j(\theta_1-\theta_2-\mu_\varphi)}]$. Hence the joint distribution of two neighboring phases can be written as

$$\begin{aligned}p(\theta_1,\theta_2)&=\pi^{-2}|\det(\mathbf{\Phi})|\int_0^\infty\int_0^\infty r_1r_2\exp[-(r_1^2\varphi_{11}+r_2^2\varphi_{22})]\\&\quad\times\exp(-2r_1r_2|\varphi_{12}|\cos(\theta_1-\theta_2-\mu_\varphi))\,dr_1\,dr_2\\&=\frac{1-\lambda^2}{4\pi^2(1-c^2)}\left[1-\frac{c\cos^{-1}(c)}{\sqrt{1-c^2}}\right],\end{aligned} \tag{5}$$

where $c=\lambda\cos(\theta_1-\theta_2-\mu+\pi)$, the correlation coefficient $\lambda=|\varphi_{12}|/\sqrt{\varphi_{11}\varphi_{22}}=|\psi_{12}|/\sqrt{\psi_{11}\psi_{22}}$, $\mu=\angle\psi_{12}=\mu_\varphi+\pi$, and $\angle$ denotes phase. Fig. 1 shows that behaviors of the model (5) look very similar to the empirical joint distribution of neighboring phases.

2.4. Vonn distribution of relative phases

A relative phase at a spatial location (i,j) within a particular complex subband is defined as the phase difference of two adjacent complex wavelet coefficients [31], e.g.,

$$\theta(i,j)=\angle z(i,j)-\angle z(i,j+1),$$

$$\text{or}\quad\theta(i,j)=\angle z(i,j)-\angle z(i+1,j), \tag{6}$$

where $z(i,j)$ is the coefficient at position (i,j). It is noted that to handle circularity of phases, $\angle z$ returns the phase angle, in radian, for complex coefficient z. The angles lie between $\pm\pi$.

Theorem 2.1. *If the coefficients in a complex wavelet subband are characterized by a complex Gaussian, then the*

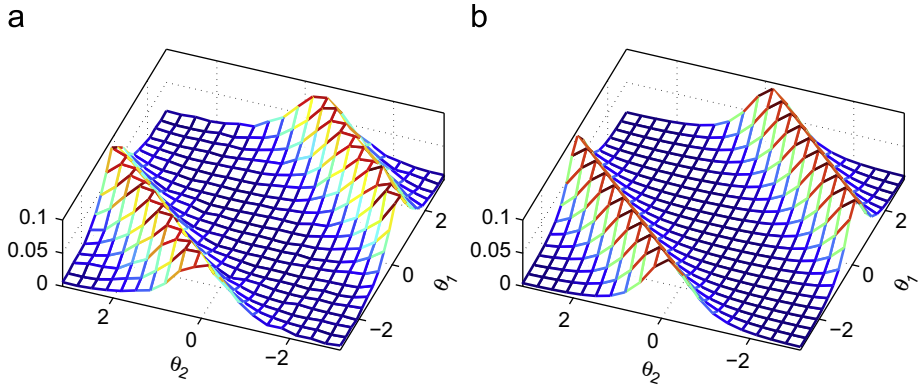

Fig. 1. The empirical joint distribution of two neighboring phases and the joint density function with $\mu=0.15,\lambda=0.74$ at a particular complex wavelet subband in the curvelet domain for the texture image 'Misc.0002'. (a) Empirical distribution and (b) model.

probability density function for relative phases of complex coefficients in this subband will be

$$p(\theta)=\frac{1-\lambda^2}{2\pi(1-c^2)}\left[1-\frac{c\cos^{-1}(c)}{\sqrt{1-c^2}}\right], \tag{7}$$

where $c=\lambda\cos(\theta-\mu+\pi)$, $-\pi\le\theta,\mu\le\pi$, *and* $0\le\lambda\le 1$.

Proof. If the coefficients in a complex wavelet subband are characterized by a complex Gaussian, the joint distribution $p(\theta_1,\theta_2)$ is given in (5). A relative phase can be considered as $\theta=\theta_1-\theta_2$, where θ_1 is the phase of the reference coefficient at location (i,j) and θ_2 is the phase of the nearest neighbor coefficient at location $(i,j+1)$ or $(i+1,j)$. Therefore, the distribution of relative phases θ is given by a pdf which we called Vonn distribution as follows:

$$p(\theta)=\int_{-\pi}^{\pi}p_\Theta(\theta+\theta_2,\theta_2)\,d\theta_2=\frac{1-\lambda^2}{2\pi(1-c^2)}\left[1-\frac{c\cos^{-1}(c)}{\sqrt{1-c^2}}\right]. \qquad \square$$

The Vonn density function of relative phases θ in (7) with various values of λ and μ are depicted in Fig. 2. The Vonn distribution is unimodal with two parameters μ and λ, and is symmetrical about $\theta=\mu$. μ is the mean direction and λ is the correlation parameter. The larger the value of the correlation parameter λ, the denser the clustering around μ. Note that $p(\theta;\mu,\lambda)$ and $p(\theta+\pi;\mu,-\lambda)$ are the same distribution. For our model, we set the values of λ to be non-negative, and the range of θ is $[-\pi\ \ \pi]$. It is noted that the range of usual principal value of $\arccos(c)$ is $[0\ \ \pi]$. The maximum-likelihood (ML) estimator for the Vonn distribution will be discussed in Section 4.

3. Derivation of the Vonn distribution of relative phases based on Gaussian scale mixture model

In Section 2, we proposed the density function in (7) for relative phases within a particular subband with the assumption that the distributions of real and imaginary coefficients are Gaussian. However, this assumption is often not realistic. A more widely acceptable model is Gaussian scale mixture (GSM) [8], which is a product of a real Gaussian random vector and an independent hidden random scalar multiplier. Real wavelet coefficients are linked indirectly by their shared dependency on a hidden multiplier. Hence, the GSM model can describe the shape of real wavelet coefficient distributions and the correlation between neighbor coefficients. In this section, we will derive a probability density function for relative phases with the assumption that real and imaginary coefficients are modeled by two GSM models [8,13,36].

3.1. Complex Gaussian scale mixture for complex coefficients

The complex directional filters produce real coefficients $\mathbf{x}$ and imaginary coefficients $\mathbf{y}$ which are characterized by a GSM model. It is assumed that $\mathbf{x}\triangleq\sqrt{\nu}\mathbf{u}_r$ and $\mathbf{y}\triangleq\sqrt{\nu}\mathbf{u}_i$. Then $\mathbf{z}\triangleq\sqrt{\nu}\mathbf{u}$, where $\mathbf{z}=\mathbf{x}+j\mathbf{y}$ and $\mathbf{u}=\mathbf{u}_r+j\mathbf{u}_i$. Since the distribution of the real part $\mathbf{x}$ is GSM, $p(\mathbf{x}|\nu)$ is Gaussian. Similarly for the imaginary part $\mathbf{y}$, $p(\mathbf{y}|\nu)$ is also Gaussian. Thus from Section 2.1, the distribution of complex wavelet coefficients $\mathbf{z}$ will be complex Gaussian when it is conditioned on ν as follows:

$$p(\mathbf{z}|\nu)=\frac{\exp(-\mathbf{z}^H\mathbf{C}_{z|\nu}^{-1}\mathbf{z})}{(\pi)^N\det(\mathbf{C}_{z|\nu})}, \tag{8}$$

where the covariance matrix $\mathbf{C}_{\mathbf{z}|\nu}=\nu\mathbf{C}_\mathbf{u}$, $\mathbf{C}_u=E[\mathbf{u}\mathbf{u}^H]$ is the complex covariance matrix of $\mathbf{u}$, and N is the dimensionality of $\mathbf{z}$ and $\mathbf{u}$.

The distribution of vector $\mathbf{u}$ is a complex Gaussian and the scalar real variable $\sqrt{\nu}$ has some distribution on $(0,\infty)$ with a density $p(\nu)(\nu>0)$. $\mathbf{z}\triangleq\sqrt{\nu}\mathbf{u}$ is referred as the scale mixtures of complex Gaussians (CGSM) [37] as follows:

$$p_\mathbf{z}(\mathbf{z})=\int\frac{\exp(-\mathbf{z}^H(\nu\mathbf{C}_u)^{-1}\mathbf{z})}{(\pi)^N\det(\nu\mathbf{C}_u)}p(\nu)\,d\nu. \tag{9}$$

Similar to the GSM model, the probability density of the multiplier ν can be found as in [13].

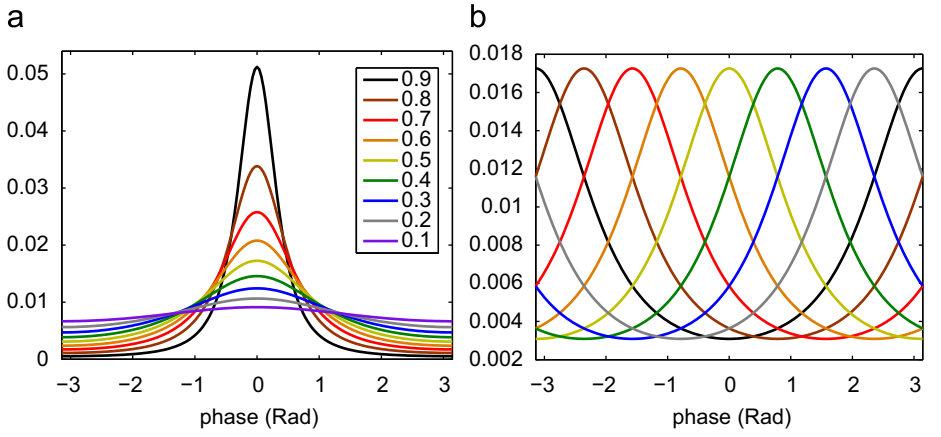

Fig. 2. Distributions of relative phases: (a) $\lambda=[0.1,0.2,\ldots,0.9]$ and $\mu=0$, (b) $\lambda=0.5$ and $\mu=[-\pi,-3\pi/4,\ldots,3\pi/4]$.

3.2. Joint distribution of two neighboring phases

The coefficients $\mathbf{z}=\mathbf{x}+j\mathbf{y}$ within each local neighborhood around a reference coefficient of a complex subband are characterized by a CGSM model. Now we consider the case of N=2 with $\mathbf{z}=(z_1,z_2)^T$ and

$$p(r_1,r_2,\theta_1,\theta_2|\nu)=r_1r_2\frac{\exp(-\mathbf{z}^H\mathbf{C}_{z|\nu}^{-1}\mathbf{z})}{(\pi)^2\det(\mathbf{C}_{z|\nu})}, \tag{10}$$

where $z_n=r_ne^{j\theta_n}$, n = 1,2, and the covariance $\mathbf{C}_{z|\nu}=E[\mathbf{z}\mathbf{z}^H|\nu]=\nu\mathbf{C}_{\mathbf{u}}=\nu[\begin{smallmatrix}\psi_{11} & \psi_{12}\\ \psi_{12}^* & \psi_{22}\end{smallmatrix}]=\mathbf{\Phi}^{-1}$.

Hence the joint density of neighboring phases when conditioned on ν can be written as

$$\begin{aligned}p(\theta_1,\theta_2|\nu)&=\pi^{-2}|\det(\mathbf{\Phi})|\int_0^\infty\int_0^\infty r_1r_2\exp[-(r_1^2\varphi_{11}+r_2^2\varphi_{22})]\\&\quad\times\exp(-2r_1r_2|\varphi_{12}|\cos(\theta_1-\theta_2-\mu_\varphi))\,dr_1\,dr_2\\&=\frac{1-\lambda^2}{4\pi^2(1-c^2)}\left[1-\frac{c\cos^{-1}(c)}{\sqrt{1-c^2}}\right],\end{aligned}$$

where $c=\lambda\cos(\theta_1-\theta_2-\mu+\pi)$, $\lambda=|\varphi_{12}|/\sqrt{\varphi_{11}\varphi_{22}}=|\nu\psi_{12}|/\sqrt{\nu^2\psi_{11}\psi_{22}}$ and $\mu=\angle\nu\psi_{12}=\mu_\varphi+\pi$. Since ν is real and non-negative, λ and μ are independent from ν. Hence

$$p(\theta_1,\theta_2)=\int p(\theta_1,\theta_2|\nu)p(\nu)\,d\nu=\frac{1-\lambda^2}{4\pi^2(1-c^2)}\left[1-\frac{c\cos^{-1}(c)}{\sqrt{1-c^2}}\right].$$

3.3. Vonn distribution of relative phases

Theorem 3.1. *If the coefficients in a complex wavelet subband are characterized by the scale mixtures of complex Gaussians (CGSM), then the probability density function for relative phases of complex coefficients in this subband will be*

$$p(\theta)=\frac{1-\lambda^2}{2\pi(1-c^2)}\left[1-\frac{c\cos^{-1}(c)}{\sqrt{1-c^2}}\right], \tag{11}$$

where $c=\lambda\cos(\theta-\mu+\pi)$, $-\pi\le\theta,\mu\le\pi$ *and* $0\le\lambda\le1$.

Proof. When the coefficients of a complex subband are characterized by a complex Gaussian or a CGSM model, the joint distributions of neighboring phases in (5) and in (11) are identical and independent from ν. So the distribution of relative phases shown in (7) is also true with the assumption of CGSM model.

The Vonn distribution in (7) fits very well with the distribution of relative phases in complex subbands. Fig. 3 shows an empirical relative phase histogram in a particular complex wavelet subband for three different images, along with the best fitting of the Vonn distribution. Fitting was performed by maximizing the likelihood function of relative phase samples within a subband (see Section 4).

We also show the relative entropy ΔH (KLD) between the histogram and the model divided by the histogram entropy H in Table 1. It is clear that the Vonn distribution fits very well in the 40 Vistex textures with the size of 256×256, the Lena and Fingerprint images with the average of $\Delta H/H=0.0007$, 0.0008 and 0.0003, respectively. For other images in Table 1, the performance of the fitted model is still acceptable with $\Delta H/H<0.0027$. It is noted that the images in Fig. 3 and Table 1 are decomposed by the uniform discrete curvelet transform (UDCT). The UDCT in our simulations has four

Table 1
Average relative entropy of Vonn model and histogram, as a fraction of the total entropy of the histogram ($\Delta H/H$) in curvelet domain.

Texture (Vistex)	Subbands	Subband size	Bins	$\Delta H/H$
640 subimages	3840	64×64	32	0.0021
40 subimages	240	128×128	64	0.0011
40 images	240	256×256	128	0.0006
Lena	6	256×256	128	0.0007
Barbara	6	256×256	128	0.0026
Boat	6	256×256	128	0.0015
Fingerprint	6	256×256	128	0.0003
Peppers	6	128×128	64	0.0015
House	6	128×128	64	0.0027
Cameraman	6	128×128	64	0.0019

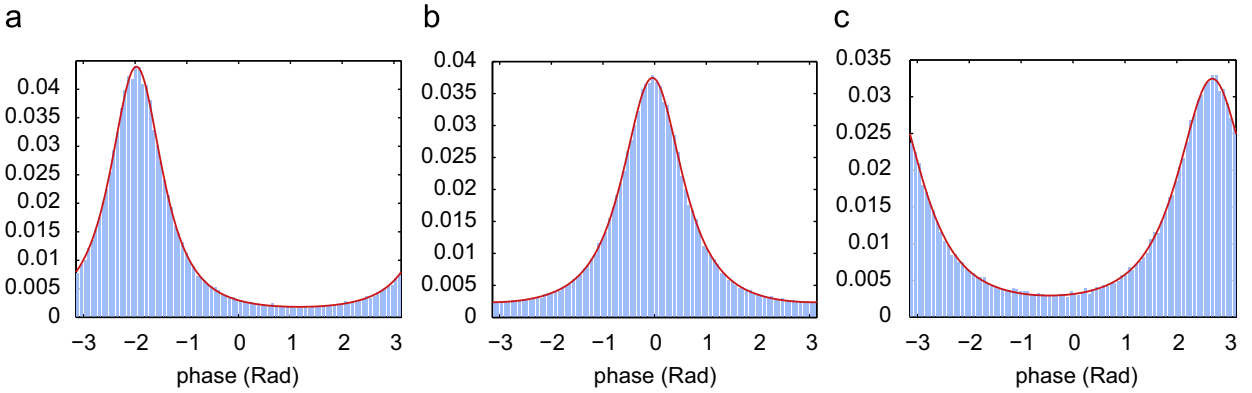

Fig. 3. Vonn distributions of relative phases fitted to empirical histograms at a particular finest complex wavelet subband. Below each plot are the estimated parameter values, and the relative entropy ΔH (Kullback–Leibler divergence—KLD) between the histogram and the model, as a fraction of the histogram entropy H (with 90 bins). (a) Fabric.0017, $[\mu,\lambda]=[-1.98,0.77]$, $\Delta H/H=0.00018$, (b) Stone.004, $[\mu,\lambda]=[-0.04,0.71]$, $\Delta H/H=0.00009$, and (c) Brick0004, $[\mu,\lambda]=[2.68,0.64]$, $\Delta H/H=0.00023$.

directional scales, with $N = 6$ at each scale. It is a modified version of discrete curvelet transform [38]. For detailed construction of the UDCT, the reader is referred to [39].

3.4. An extension of definition for relative phase

In this section, we extend the definition of relative phase and prove that the Vonn distribution can be used to model for general relative phase. The relative phase is the phase difference of two complex wavelet coefficients within a local neighboring in the same subband or in two different subbands. The previous definition [31] in Section 2.4 is a special case when two complex coefficients are adjacent. In the general case, the relative phase can be given by

$$\theta(i,j) = \angle z(i,j) - \angle z(i+d_i, j+d_j), \tag{12}$$

where $z(i,j)$ is the coefficient at position (i,j), and d_i, d_j are the distances between two coefficients in row and in column, respectively, e.g., $d_i = 4$, $d_j = 0$, or $d_i = 2$, $d_j = 8$.

In Eq. (10), if θ_1 is the phase of a reference phase at location (i,j), and θ_2 is the phase of a neighboring coefficient at location $(i+d_i,j+d_j)$, then the relative phase, $\theta = \theta_1 - \theta_2$, has the probability density function as in (11). Some histograms of relative phase in the same subband and fitted models corresponding to various values of distance d_j are shown in Fig. 4(a)–(c). When the distance d_j increases, the correlation parameter λ decreases, and vice versa. This conclusion is consistent with the correlation between two coefficients. If the distance d_j is smaller, the correlation between them is higher. Therefore λ is larger and the relative phases clustering around μ is denser. The distribution in Fig. 4(c) with $d_j = 4$ is flatter than the distributions with $d_j = 1$ and 2 in Fig. 4(a) and (b), respectively. We also show the histogram of relative phase for parent and children coefficients in two scales at the same direction and fitted model in Fig. 4(d). The Vonn distribution in (11) fits well with the distribution of relative phases with different distances d_j in the same subband as well as in two different subbands.

4. Maximum likelihood estimator for Vonn distribution of relative phase

In this section we describe how to estimate two parameters of the Vonn distribution using the maximum-likelihood estimator (ML). Let $\theta_1, \theta_2, \ldots, \theta_n$ be a set of observations from a Vonn distribution with parameters μ and λ, then $\theta_1, \theta_2, \ldots, \theta_n$ are i.i.d. with pdf

$$p(\theta) = \frac{1-\lambda^2}{2\pi(1-c^2)}\left[1 - \frac{c\cos^{-1}(c)}{\sqrt{1-c^2}}\right], \tag{13}$$

where $c = \lambda\cos(\theta - \mu + \pi)$.

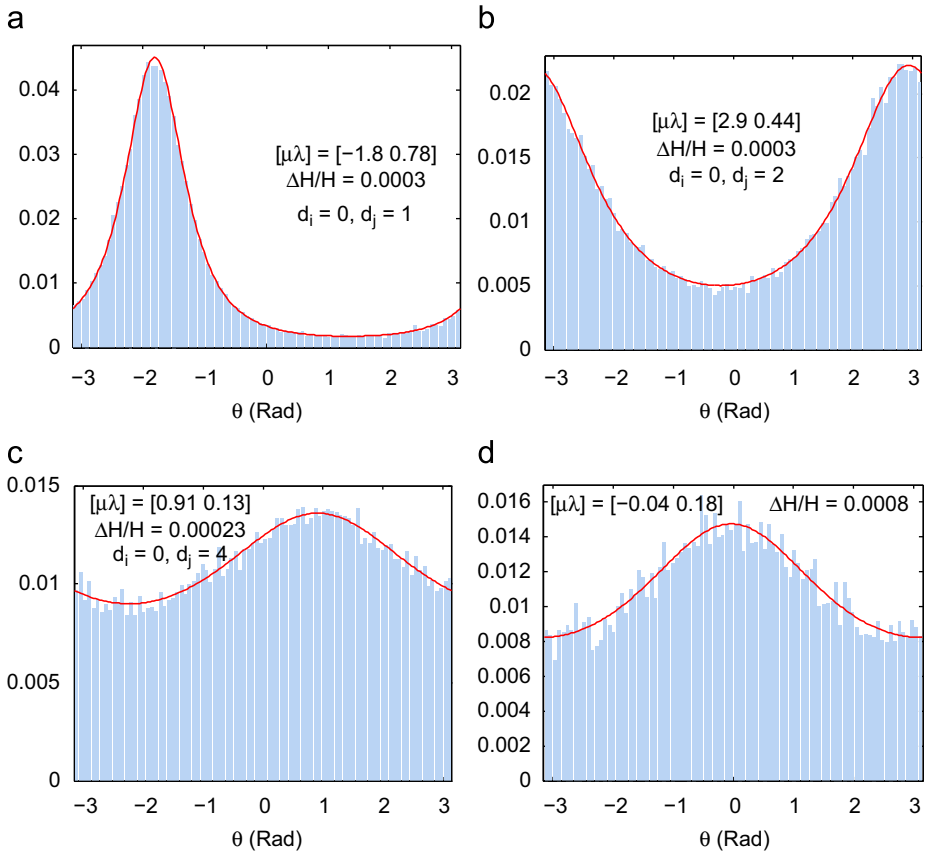

Fig. 4. Vonn distribution of relative phase fitted to the empirical histograms at a particular finest complex wavelet subband of fingerprint image. In each plot, the estimated parameter values, and the relative entropy $\Delta H/H$ are shown. (a) RP (d=1), (b) RP (d=2), (c) RP (d=4) and (d) RP (parent and children).

The likelihood function is given by

$$L(\mu,\lambda|\theta_1,\theta_2,\ldots,\theta_n)=\prod_{i=1}^{n}p(\theta_i;\mu,\lambda), \tag{14}$$

and its logarithm

$$l(\mu,\lambda|\theta_1,\theta_2,\ldots,\theta_n)=\log L, \tag{15}$$

where μ and λ are parameters to be estimated as follows:

$$[\hat{\mu}\ \ \hat{\lambda}]=\text{argmax}_{[\mu\ \ \lambda]}\sum_{i=1}^{n}\log p(\theta_i;\mu,\lambda), \tag{16}$$

$$\hat{\lambda}=\text{argmax}_{\lambda}\sum_{i=1}^{n}\log p(\theta_i;\mu,\lambda). \tag{17}$$

Differentiating (15) with respect to μ and λ, and equating to zero, we obtain the likelihood equations

$$f(\mu)=\frac{\partial l(\mu,\lambda|\theta_1,\theta_2,\ldots,\theta_n)}{\partial\mu}=0, \tag{18}$$

$$g(\lambda)=\frac{\partial l(\mu,\lambda|\theta_1,\theta_2,\ldots,\theta_n)}{\partial\lambda}=0. \tag{19}$$

These equations can be solved numerically to find the parameters μ and λ. However, it should be noted that the parameter μ can be also estimated by the mean direction

$$\hat{\mu}=\arctan\frac{\sum_{i=1}^{n}\sin(\theta_i)}{\sum_{i=1}^{n}\cos(\theta_i)}, \tag{20}$$

where arctan is the four-quadrant inverse tangent. Therefore, to simplify the estimation problem, we propose using mean direction to estimate μ and using the Newton Raphson iterative method to find solution for $g(\lambda)=0$ with $\mu=\hat{\mu}$.

Substitute $\hat{\mu}$ into (19), the Newton iteration can be stated as

$$\lambda^{[k+1]}=\lambda^{[k]}-\frac{g(\lambda^{[k]})}{g'(\lambda^{[k]})}. \tag{21}$$

We derive $g(\lambda)$ and $g'(\lambda)$ in Appendix A. They are given by

$$g(\lambda)=\sum_{i=1}^{n}h(\lambda,-1)+h(\lambda,+1)-1.5[h(\lambda,-x_i)+h(\lambda,x_i)]+\frac{b'(\lambda,x_i)}{b(\lambda,x_i)}, \tag{22}$$

$$g'(\lambda)=\sum_{i=1}^{n}-[h^2(\lambda,-1)+h^2(\lambda,+1)]+1.5[h^2(\lambda,-x_i)+h^2(\lambda,x_i)]+\frac{b''b'-b'^2}{b^2(\lambda,x_i)}, \tag{23}$$

where

$$x_i=\cos(\theta_i-\hat{\mu}+\pi),\quad h(\lambda,x_i)=\frac{x_i}{1+\lambda x_i}, \tag{24}$$

$$b(\lambda,x_i)=\sqrt{1-\lambda^2x_i^2}-\lambda x_i\cos^{-1}(\lambda x_i), \tag{25}$$

$$b'(\lambda,x_i)=-x_i\cos^{-1}(\lambda x_i)$$

and

$$b''(\lambda,x_i)=\frac{x_i^2}{\sqrt{1-\lambda^2x_i^2}}. \tag{26}$$

We propose using the correlation coefficient as a good initial value for the root of $g(\lambda)$ as follows:

$$\lambda^{[0]}=\frac{|\psi_{12}|}{\sqrt{\psi_{11}\psi_{22}}}, \tag{27}$$

where the covariance of complex wavelet coefficients in a subband is $\mathbf{C}_z=[\begin{smallmatrix}\psi_{11} & \psi_{12}\\ \psi_{12} & \psi_{22}\end{smallmatrix}]$.

With the initial value $\lambda^{[0]}$ as in (27), our ML estimator converges with a few number of iterations. In a practical implementation, we fit 3840 subbands using the ML estimator. The simulation results showed that the average number of iterations is around 5, and it takes about 0.03 (s) to estimate two Vonn parameters. To verify the accuracy of Eq. (20), we generate a Vonn random variable with two known parameters and use Eq. (20) to estimate μ. The error is less than 0.1%. It is possible to solve for both parameters by numerical method. However, the number of iterations to solve for both parameters is higher than for one and the time to estimate two parameters is also higher because more computations are involved.

5. A comparison of von Mises, wrapped Cauchy and Vonn distributions for relative phase

In this section, the Vonn distribution is compared with von Mises and wrapped Cauchy distributions which have been proposed for relative phases in [31]. We also evaluate the Vonn distribution for different complex wavelet transforms including dual-tree complex wavelets (DTCWT) [40], complex directional filter banks (CDFB) [30] and uniform discrete curvelet transform (UDCT) [39].

5.1. Von Mises distribution

An angular random variable θ has the von Mises distribution (VM) with the parameters μ and v $VM(\mu,v)$ [41,42] if its probability density function (PDF) has the form

$$p(\theta;\mu,v)=\frac{1}{2\pi I_0(v)}e^{v\cos(\theta-\mu)}, \tag{28}$$

where I_0 denotes the modified Bessel function of the first kind and the zero-th order which can be defined by $I_0(v)=(1/\pi)\int_0^{\pi}e^{v\cos\theta}d\theta$. The von Mises density functions in (28) with various values of v are depicted in Fig. 5(a). The parameters of the von Mises distribution are estimated using maximum-likelihood as in [41].

5.2. Wrapped Cauchy distribution

The wrapped Cauchy (WC) distribution is obtained by wrapping the Cauchy distribution on the real line with density around the circle. It has the probability density function [41,42]

$$p(\theta)=\frac{1}{2\pi}\frac{1-\rho^2}{1+\rho^2-2\rho\cos(\theta-\mu)},\quad -\pi\le\theta\le\pi, \tag{29}$$

where $\rho=e^{-\sigma}$. The wrapped Cauchy density functions in (28) with various values of ρ are depicted in Fig. 5(b). The maximum likelihood estimation for this model can be obtained by a recursive algorithm [42].

5.3. Comparison results

The von Mises, wrapped Cauchy and Vonn distributions fit well with the marginal distribution of the RPs at a subband of the Lena image shown in the first row of Fig. 6 with $\Delta H/H = 0.0009, 0.0008$ and 0.0002, respectively. However, for a subband of the Boat image, the von Mises distribution cannot capture the peaky and heavy-tailed distribution as shown in the second row of Fig. 6 with $\Delta H/H = 0.0209$. While the Vonn model precisely describes the histogram of relative phase with $\Delta H/H = 0.001$. For both examples, the wrapped Cauchy distribution is rather accurate to capture the histograms of relative phases. However, when compared with the Vonn model, the wrapped Cauchy model is less precise. The Vonn fitting was performed by maximizing a likelihood function proposed in Section 4. In Fig. 6, the images are decomposed by the UDCT transform.

We also evaluate three relative phase distributions for many real images including texture images as well as standard images, which are decomposed by various complex wavelet transforms such as the DTDWT [40], CDFB [30] and UDCT [39]. The data for evaluation and their information such as the number of subbands, size of subband and number of bins are in Table 1. The simulation results in Table 2 show that for most of the

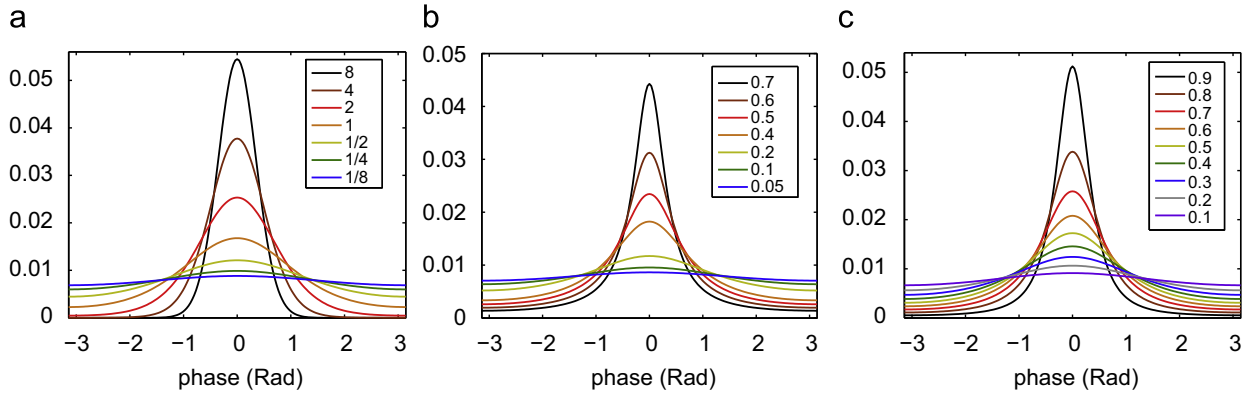

Fig. 5. (a) Von Mises distribution with $\nu = [1/8, 1/4, \ldots 8]$, (b) wrapped Cauchy distribution with $\rho = [0.05, 0.1, \ldots 0.7]$, and (c) Vonn distribution with $\lambda = [0.1, 0.2, \ldots, 0.9]$.

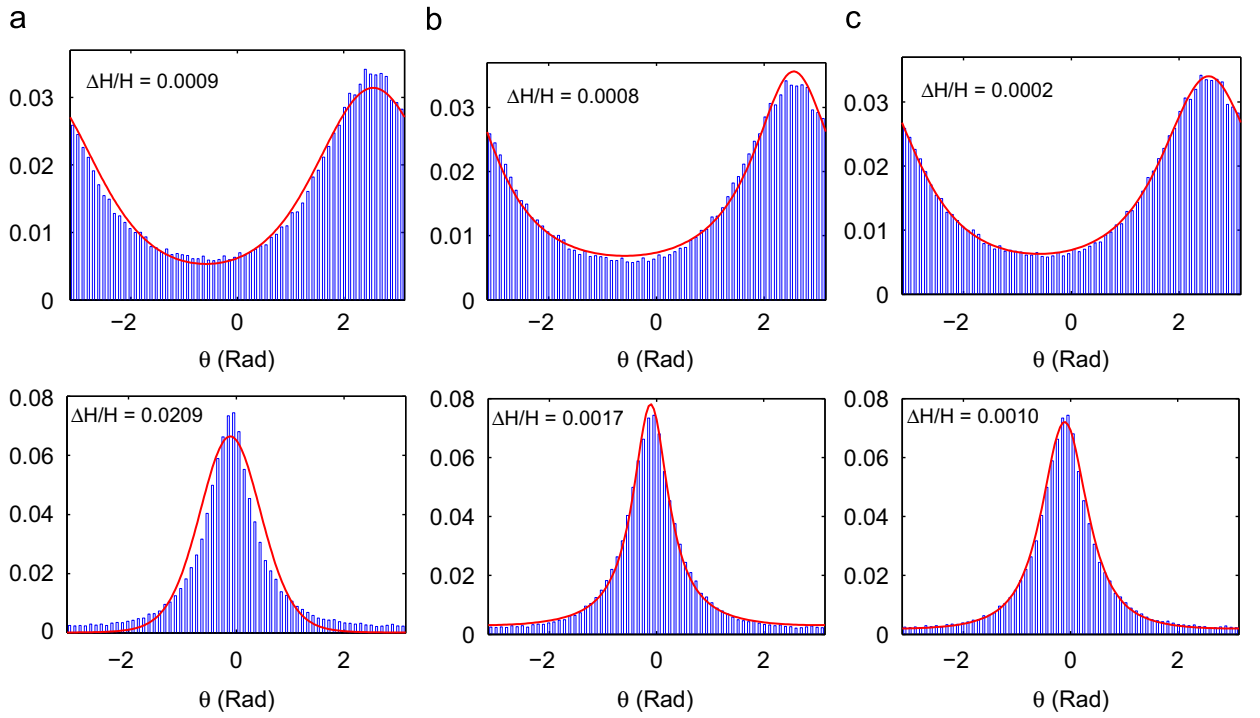

Fig. 6. Circular distributions fitted to the empirical histograms of relative phase at a particular finest complex wavelet subband. In each plot, the relative entropy $\Delta H/H$ are shown. The first row is the Lena image, and the second one is the Boat image. (a) Von Mises, (b) wrapped Cauchy and (c) Vonn.

tested images, the Vonn model is much more accurate than the von Mises and wrapped Cauchy distributions. For only several images, the accuracy of the Vonn model approximates the von Mises.

We observe that the von Mises distribution only fits very well with the relative phase pdf which has the Gaussian shape and the wrapped Cauchy only fits very well with the relative phase pdf which has the peaky and heavy-tailed shape, while the Vonn distribution do well both peaky, heavy-tailed and Gaussian-shaped pdfs. The last row in Table 2 presents the average $\Delta H/H$ of all tested images. It is clear that compared with the von Mises and the wrapped Cauchy distributions, the Vonn distribution is much better in fitting model for relative phase of complex wavelet coefficients.

Table 2
Average relative entropy of model and histogram ($\Delta H/H$) for Von Mises, wrapped Cauchy and Vonn distributions in various complex wavelet domains.

Texture (Vistex)	Von Mises	Wrapped Cauchy	Vonn
Dual-tree complex wavelet transform			
640 subimages	0.0042	0.0027	**0.0024**
40 subimages	0.0028	0.0015	**0.0014**
40 images	0.0020	0.0010	**0.0008**
Lena	**0.0006**	0.0011	0.0008
Barbara	**0.0013**	0.0017	**0.0013**
Boat	**0.0020**	0.0025	0.0023
Fingerprint	0.0014	0.0007	**0.0003**
Peppers	**0.0013**	0.0020	0.0016
House	0.0024	0.0018	**0.0017**
Cameraman	**0.0019**	0.0022	0.0020
Complex directional filter bank			
640 subimages	0.0139	0.0065	**0.0033**
40 subimages	0.0110	0.0042	**0.0016**
40 images	0.0086	0.0029	**0.0009**
Lena	0.0024	0.0022	**0.0006**
Barbara	0.0026	0.0042	**0.0023**
Boat	0.0044	0.0031	**0.0013**
Fingerprint	0.0098	0.0029	**0.0004**
Peppers	0.0045	0.0028	**0.0020**
House	**0.0043**	0.0073	0.0046
Cameraman	0.0033	0.0025	**0.0012**
Uniform discrete curvelet transform			
640 subimages	0.0103	0.0045	**0.0021**
40 subimages	0.0078	0.0031	**0.0011**
40 images	0.0060	0.0024	**0.0006**
Lena	0.0015	0.0015	**0.0007**
Barbara	**0.0023**	0.0047	0.0026
Boat	0.0041	0.0019	**0.0015**
Fingerprint	0.0092	0.0029	**0.0003**
Peppers	0.0029	0.0023	**0.0015**
House	**0.0019**	0.0052	0.0027
Cameraman	0.0043	0.0027	**0.0019**

5.4. Range of estimated parameter in Vonn model

It is of interest to know the common range for the values of λ in Vonn model for texture images as well as of v in von Mises model and of ρ in wrapped Cauchy model. Fig. 7 shows the histograms of the estimated parameters for 3840 finest subbands of size 64×64 from 640 texture images of size 128×128 described in Section 6.3. When the UDCT is used to decompose texture images, most of estimated von Mises model parameters v parameter are from around 1 to 3. The ρ values of the wrapped Cauchy model are from 0.45 to 0.65, while the λ values of the Vonn model are from 0.55 to 0.8.

6. Application to texture image retrieval

In this section, the Vonn model is applied to texture image retrieval. In the first experiment, a comparison of various features such as energy feature [43], GGD-based feature [44], relative phase feature [29] and our relative phase feature using Vonn distribution in texture retrieval is presented. In the second experiment, the performance of our proposed method is also compared with the performances of different state-of-the-art methods.

6.1. Proposed Vonn feature for texture image

Since the Vonn distribution fits very well with relative phase distributions of complex wavelet coefficients, we propose using the Vonn model for texture image retrieval application. Two Vonn parameters will be estimated for each subband. Fig. 8 shows two sample subimages and their extracted features μ and λ are also shown in Table 3.

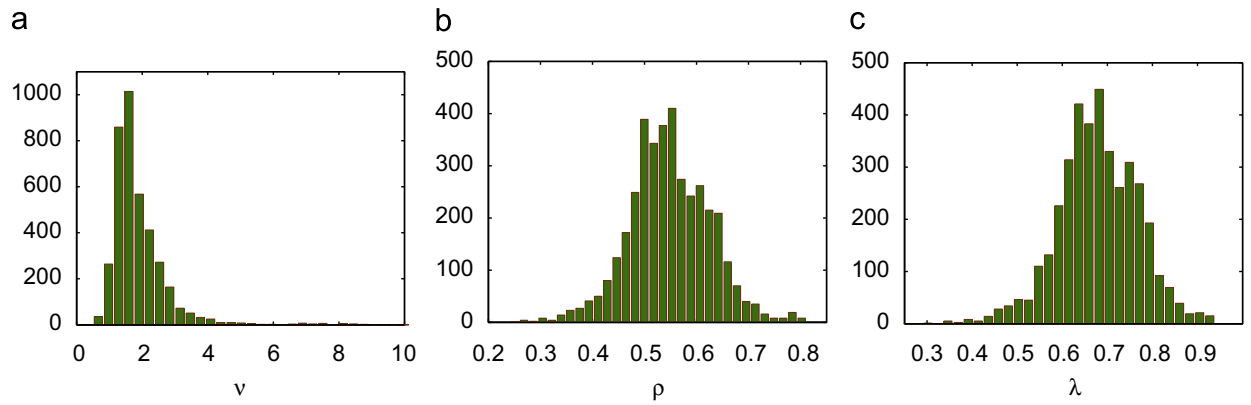

Fig. 7. Histogram of estimated values for the parameter v (von Mises), ρ (wrapped Cauchy) and λ (Vonn) of 3840 finest subbands of size 64×64 from 640 texture images of size 128×128. (a) v—Von Mises, (b) ρ—wrapped Cauchy and (c) λ—Vonn.

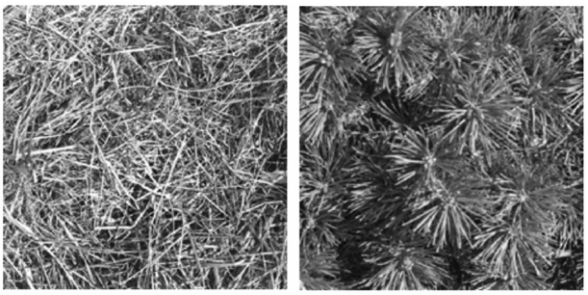

Fig. 8. Two subimages: Grass.0001 and Leaves.0010 with the size of 128×128 from the VisTex databases.

Table 3
Some examples of the proposed features using Vonn distribution.

Image	μ_4	μ_5	μ_6	λ_4	λ_5	λ_6
Grass.0001	−2.13	0.01	2.20	0.67	0.72	0.65
Leaves.0010	−1.66	0.07	1.68	0.80	0.80	0.81

Grass.0001 and Leaves.0010 images are used.

With the same subband, the images have the Vonn distributions with different parameters, e.g. at subband 4, the Grass.0001 has the center at $\mu_4 = -2.13$, while the Leaves.0010 has the center at $\mu_4 = -1.66$. The Vonn distribution of the Leaves.0010 is more peaky with the peak of 0.15 than that of the Leaves.0011 with the peak of 0.10 at subband 4. It is clear that the distinction between two different types of textures can be captured and recognized by the Vonn distribution. The proposed Vonn feature provides statistical information of relative phases for subbands and can be used to discriminate textures. Therefore, the Vonn parameters will be used as an additional feature for texture image retrieval.

6.2. Texture feature extraction

Each image in the database is decomposed by the following three decompositions: the UDCT, the 2-D Gabor transform and the CDFB. The Gabor wavelet and the UDCT are applied with four scales and six orientations per scale, while the CDFB has three scales of eight orientations. For each subband, the mean and standard deviation of absolute values of the coefficients are calculated as in [43]. The relative phase (RP) feature which includes circular means and standard deviations of relative phases are computed as in [29], the GGD features are estimated as in [44] and the GGD-WC features are estimated as in [31]. To construct the Vonn based feature vector, the relative phase matrix of each complex subband in the curvelet domain is created as in (12). For each relative phase matrix, two parameters μ and λ of the Vonn are estimated by fitting the histogram and the Vonn distribution (7). These parameters are used to form the Vonn model based feature vector.

In order to obtain a feature vector which has the same dimension as that of the Gabor [43], the CDFB-RP [29] and the GGD-WC [31], the GGD-Vonn feature vectors are formed by 12 features of the Vonn model from the finest scale, 24 features of the GGD model from the two finest scales, and 12 means of the magnitudes of curvelet coefficients from the two coarsest scales.

6.3. Texture image database and feature database

We select 40 image textures from the VisTex databases used in [44,45] for our experiments. Each of these 512×512 images is divided into sixteen 128×128 non-overlapping subimages, thus creating a database of 640 texture samples. Each original image is treated as a single class and therefore there are 16 samples from each of the 40 classes. To reduce the intensity correlation, all images are normalized to have zero mean and unit variance. For each image in the database, the UDCT curvelet transform is applied. The RP matrix of each subband is created as in (12), and their corresponding feature vectors are computed.

6.4. Distance measure and query processing

The query pattern can be any one of the texture patterns from the image database. The distances between two magnitude feature vectors and two RP feature vectors are computed as in [29] and the distance between two GGD feature vectors is computed as in [44]. The distance between two Vonn feature vectors f_x and f_y is given by

$$d(f_x,f_y) = \sum_k D_{KL}(p(.;\mu_k(x),\nu_k(x))||p(.;\mu_k(y),\nu_k(y))), \tag{30}$$

where k is the index of subbands and the Kullback–Leibler divergence D_{KL} between two PDFs $p(\theta;\mu_1,\lambda_1)$ and $p(\theta;\mu_2,\lambda_2)$ is defined as

$$D_{KL}(P_1||P_2) = \int_{-\pi}^{\pi} p(\theta;\mu_1,\lambda_1)\log\frac{p(\theta;\mu_1,\lambda_1)}{p(\theta;\mu_2,\lambda_2)}d\theta, \tag{31}$$

and a numerical method with 128 bins is applied to estimate this KLD.

For each query image, N nearest neighbors are selected, and the number of these textures belonging to the same class as the query texture, except for itself, is counted. This number (less than or equal to 15) divided by 15 is defined as the retrieval rate. The performance of the entire class is obtained by averaging this rate over the 16 members which belong to the same class of texture. The average of all classes is the overall performance of the method.

6.5. Experimental results

We compare our proposed GGD-Vonn feature using the UDCT curvelet transform with the Gabor and CDFB. In this experiment, all 24 subbands are used to form feature vectors. If only the top 15 texture images nearest to the query texture are considered, the GGD-Vonn gives the best overall retrieval performance of 85.82% as shown in Table 4. The CDFB-RP and the GGD are at 82.26% and 81.52%, while the magnitude based Gabor is at 80.81%. Fig. 9 shows that the overall performance of the

Table 4
Average retrieval accuracy of 40 VisTex texture images using various features.

	Gabor	GGD	CDFB-RP	GGD-Vonn
Feature type	m, σ	α, β m, σ	m, σ m_c, σ_c	α, β μ, λ, m
Feature length	48	48	48	48
N = 15	80.81	81.52	82.26	**85.82**

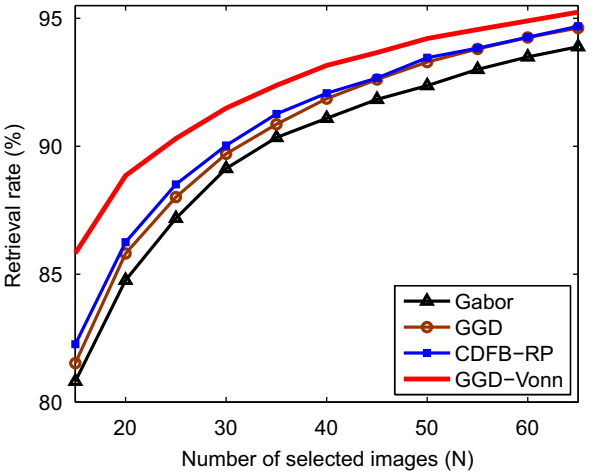

Fig. 9. Average retrieval rate according to the number of top images considered when various features are used.

Table 5
Average retrieval rates over the whole database for various existing methods.

Methods	Feature length	Rate (%)
Standard DWT: L1 + L2	18	64.83
GGD [44]	18	75.73
Scalar WD-HMM [45]	33	76.51
Vector WD-HMM [45]	41	80.05
DT-CWT + DT-RCWT [46]	80	81.16
GGD-WC [31]	48	85.64
GGD-Vonn	48	**85.82**

GGD-Vonn model is consistently better than the others. It is clear that the information gained from the Vonn phase model raises the performance of the GGD-Vonn significantly higher than those of other features.

The performance of our proposed method is also compared with the performances of different existing methods including energy based feature [46], GGD-based feature [44], WD-HMM based feature [45] and GGD-WC [31]. Simulation results in Table 5 show that our proposed method is comparable with the GGD-WC method [31] and outperforms the others. The feature vectors of all previous methods are extracted from the magnitudes or the real values of wavelet subbands, while the GGD-Vonn and GGD-WC methods exploit phases of complex coefficients and extract image information in both magnitude and phase. The incorporated phase information which is absolutely complementary to magnitude is the reason why the new feature can achieve better performance than the others.

7. Conclusion

A new probability density is proposed for modeling relative phase distributions in the complex wavelet domain with the assumptions of Gaussian as well as Gaussian scale mixture model for real coefficients. Two parameters of the new model are estimated using the maximum-likelihood estimator. The Vonn distribution captures the behaviors of relative phases from various real images including texture images as well as standard images in the complex wavelet domain quite accurately. The simulation results show that the new model is more accurate than the von Mises and wrapped Cauchy models with various complex wavelet transforms including the UDCT, the DTCWT, as well as the CDFB. Moreover, a new image feature based on the Vonn model is proposed for the texture image retrieval application. The proposed feature captures nicely directional information from texture images because a higher image retrieval accuracy is achieved by using the new feature instead of using only the magnitude or only the GGD model of real coefficients. In addition to the GGD model of real coefficients, the Vonn based phase information is incorporated to further improve the performance. The Vonn distribution exploits phase information in the complex wavelet domain and can be useful in other signal and image processing applications.

Appendix A. Derivation of $g(\lambda)$ (22) and $g'(\lambda)$ (23)

Let $x_i = \cos(\theta_i - \hat{\mu} + \pi)$. From (15), we have

$$l = \log L = \sum_{i=1}^{n} \log \frac{1-\lambda^2}{2\pi} - 1.5\log(1-\lambda^2 x_i^2) + \log[\sqrt{1-\lambda^2 x_i^2} - \lambda x_i \cos^{-1}(\lambda x_i)], \tag{32}$$

$$g(\lambda) = \frac{\partial l}{\partial \lambda} = \sum_{i=1}^{n} \frac{1}{1+\lambda} - \frac{1}{1-\lambda} - \frac{1.5x_i}{1+\lambda x_i} + \frac{1.5x_i}{1-\lambda x_i} + \frac{b'(\lambda,x_i)}{b(\lambda,x_i)} \tag{33}$$

where

$$b(\lambda,x_i) = \sqrt{1-\lambda^2 x_i^2} - \lambda x_i \cos^{-1}(\lambda x_i), \tag{34}$$

and

$$b'(\lambda,x_i) = -x_i \cos^{-1}(\lambda x_i). \tag{35}$$

$$g'(\lambda) = \sum_{i=1}^{n} -\frac{1}{(1+\lambda)^2} - \frac{1}{(1-\lambda)^2} + \frac{1.5x_i^2}{(1+\lambda x_i)^2} + \frac{1.5x_i^2}{(1-\lambda x_i)^2} + \frac{b''(\lambda,x_i)b(\lambda,x_i) - b'^2(\lambda,x_i)}{b^2(\lambda,x_i)}, \tag{36}$$

where

$$b''(\lambda,x_i) = \frac{x_i^2}{\sqrt{1-\lambda^2 x_i^2}}. \tag{37}$$

Let

$$h(\lambda,x_i)=\frac{x_i}{1+\lambda x_i}. \tag{38}$$

Substituting (38) into (33) and (36) gives (22) and (23).

References

[1] S. Mallat, A Wavelet Tour of Signal Processing, Academic Press, San Diego, 1998.
[2] E.P. Simoncelli, Handbook of Video and Image Processing, second ed., Academic Press, 2005, pp. 431–441 (Chapter 4).
[3] H.A. Chipman, E.D. Kolaczyk, R.E. Mcculloch, Adaptive Bayesian wavelet shrinkage, Journal of the American Statistical Association 92 (1997) 1413–1421.
[4] P. Moulin, J. Liu, Analysis of multiresolution image denoising schemes using generalized Gaussian and complexity priors, IEEE Transactions on Information Theory 45 (3) (1999) 909–919.
[5] E.P. Simoncelli, Bayesian denoising of visual images in the wavelet domain, in: P. Müller, B. Vidakovic (Eds.), Bayesian Inference in Wavelet Based Models, Springer-Verlag, New York, 1999, pp. 291–308 (Chapter 18).
[6] M.S. Course, R.D. Nowak, R.G. Baraniuk, Wavelet-based signal processing using hidden Markov models, IEEE Transactions on Signal Processing 46 (4) (1998) 886–902 (special issue on Wavelets and Filter Banks).
[7] J.K. Romberg, H. Choi, R.G. Baraniuk, Bayesian tree-structured image modeling using wavelet-domain hidden Markov models, IEEE Transactions on Image Processing 10 (7) (2001) 1056–1068.
[8] M.J. Wainwright, E.P. Simoncelli, Scale Mixtures of Gaussians and the Statistics of Natural Images, Advances in Neural Information Processing Systems 12 (2000) 855–861.
[9] L. Sendur, I.W. Selesnick, Bivariate shrinkage functions for wavelet-based denoising exploiting interscale dependency, IEEE Transactions on Signal Processing 50 (11) (2002) 2744–2756.
[10] S. LoPresto, K. Ramchandran, M.T. Orchard, Wavelet image coding based on a new generalized Gaussian mixture model, in: Data Compression, Snowbird, Utah, 1997.
[11] K. Mihçak, I. Kozintev, K. Ramchandran, P. Moulin, Low-complexity image denoising based on statistical modeling of wavelet coefficients, IEEE Signal Processing Letters 6 (12) (1999) 300–303.
[12] J. Portilla, E.P. Simoncelli, A parametric texture model based on joint statistics of complex wavelet coefficients, International Journal of Computer Vision 40 (1) (2000) 49–71.
[13] J. Portilla, V. Strela, M.J. Wainwright, E.P. Simoncelli, Image denoising using scale mixtures of Gaussians in the wavelet domain, IEEE Transactions on Image Processing 12 (11) (2003).
[14] A.V. Oppenheim, J.S. Lim, The importance of phase in signals, in: Proceedings of the IEEE, vol. 69, 1981, pp. 529–541.
[15] M.G.A. Thomson, Visual coding and the phase structure of natural scenes, Network: Computation in Neural Systems 10 (2) (1999) 123–132.
[16] M.C. Morrone, R.A. Owens, Feature detection from local energy, Pattern Recognition Letters 6 (5) (1987) 303–313.
[17] P. Kovesi, Image features from phase congruency, Videre: A Journal of Computer Vision Research 1 (3) (1999) 2–26.
[18] P. Kovesi, Phase congruency: a low-level image invariant, Psychological Research 64 (2) (2000) 136–148.
[19] M.C. Morrone, D.C. Burr, Feature detection in human vision: a phase-dependent energy model, Proceedings of the Royal Society of London. Series B, Biological Sciences 235 (1988) 221–245.
[20] K. Chaudhury, M. Unser, On the shiftability of dual-tree complex wavelet transforms, IEEE Transactions on Signal Processing 58 (1) (2010) 221–232.
[21] J.G. Daugman, High confidence visual recognition of persons by a test of statistical independence, IEEE Transactions on Pattern Analysis and Machine Intelligence 15 (11) (1993) 1148–1161.
[22] D. Zhang, W.-K. Kong, J. You, M. Wong, Online palmprint identification, IEEE Transactions on Pattern Analysis and Machine Intelligence 25 (9) (2003) 1041–1050.
[23] B. Zhang, S. Shan, X. Chen, W. Gao, Histogram of Gabor phase patterns (HGPP): a novel object representation approach for face recognition, IEEE Transactions on Image Processing 16 (1) (2007) 57–68.
[24] Z. Wang, E.P. Simoncelli, Local phase coherence and the perception of blur, Advances in Neural Information Processing Systems, vol. 16, MIT Press, 2004, pp. 786–792.
[25] R. Anderson, N. Kingsbury, J. Fauqueur, Coarse-level object recognition using interlevel products of complex wavelets, in: Proceedings of IEEE International Conference on Image Processing (ICIP'05), vol. 1, 2005, pp. 3066–3077.
[26] X. Zhang, Y. Jia, Face recognition with local steerable phase feature, Pattern Recognition Letters 27 (16) (2006) 1927–1933.
[27] M. Miller, N. Kingsbury, Statistical image modelling using interscale phase relationships of complex wavelet coefficients, in: Proceedings of IEEE International Conference on Acoustics, Speech and Signal Processing (ICASSP'06), vol. 2, 2006, pp. II-789–II-792.
[28] J.F. Ryan Anderson, N. Kingsbury, Determining multiscale image feature angles from complex wavelet phases, in: Proceedings of International Conference on Image Analysis and Recognition (ICIAR), 2005, pp. 490–498.
[29] A. Vo, S. Oraintara, T.T. Nguyen, Using phase and magnitude information of the complex directional filter bank for texture image retrieval, in: Proceedings of IEEE International Conference on Image Processing (ICIP'07), vol. 4, 2007, pp. IV-61–IV-64.
[30] T.T. Nguyen, S. Oraintara, The shiftable complex directional pyramid, part 1: theoretical aspects, IEEE Transactions on Signal Processing 56 (10) (2008) 4651–4660.
[31] A. Vo, S. Oraintara, A study of relative phase in complex wavelet domain: property, statistics and applications in texture image retrieval and segmentation, Signal Processing Image Communication 25 (2010) 28–46.
[32] A. Vo, S. Oraintara, T.T. Nguyen, Statistical image modeling using distribution of relative phases in the complex wavelet domain, in: Proceedings of the 16th European Signal Processing Conference (EUSIPCO'08), 2008.
[33] N. Kingsbury, Complex wavelets for shift invariant analysis and filtering of signals, Journal of Applied and Computational Harmonic Analysis 10 (3) (2001) 234–253.
[34] N.R. Woodman, Statistical analysis based on a certain multivariate complex Gaussian distribution, The Annals of Mathematical Statistics 34 (1) (1963) 152–177.
[35] K.S. Miller, Complex Gaussian processes, SIAM Review 11 (4) (1969) 544–567.
[36] D. Andrews, C. Mallows, Scale mixtures of normal distributions, Journal of the Royal Statistical Society 36 (1) (1974) 99–102.
[37] Y. Rakvongthai, A. Vo, S. Oraintara, Complex Gaussian scale mixtures of complex wavelet coefficients, IEEE Transactions on Signal Processing, 58 (7) (2010) 3545–3556.
[38] E. Candès, L. Demanet, D. Donoho, L. Ying, Fast discrete curvelet transforms, Multiscale Modeling Simulation 5 (3) (2006) 861–899.
[39] T.T. Nguyen, H. Chauris, Uniform discrete curvelet transform for seismic processing, in: EAGE Conference and Exhibition (EAGE'08), 2008, pp. 5495–5498.
[40] N. Kingsbury, Image processing with complex wavelets, Philosophical Transactions on Royal Society London A 357 (1760) (1999) 2543–2560.
[41] K.V. Mardia, P.E. Jupp, Directional Statistics, John Wiley and Sons, 2000.
[42] S. Jammalamadaka, A. SenGupta, Topics in Circular Statistics, World Scientific, 2001.
[43] B. Manjunath, W. Ma, Texture features for browsing and retrieval of image data, IEEE Transactions on Pattern Analysis and Machine Intelligence 18 (8) (1996) 837–842.
[44] M.N. Do, M. Vetterli, Wavelet-based texture retrieval using generalized Gaussian density and Kullback–Leibler distance, IEEE Transactions on Image Processing 11 (2) (2002) 146–158.
[45] M.N. Do, M. Vetterli, Rotation invariant texture characterization and retrieval using steerable wavelet-domain hidden Markov models, IEEE Transactions on Multimedia 4 (4) (2002) 517–527.
[46] M. Kokare, P.K. Biswas, B.N. Chatterji, Texture image retrieval using new rotated complex wavelet filters, IEEE Transactions on Systems, Man and Cybernetics 35 (6) (2005) 1168–1178.